Supplementary information

Effects of magnetism and size of nano-oxide inclusions on the thermoelectric properties of $Ge_{0.96}Bi_{0.06}Te$

Can Zhu,[a] Jian Wang,[a] Xinqiang Zhu,[a] Shun Zhang,[a] Feng Xu,[a] Feng Luo,[a] Jiafu Wang,[a,b] Yan Zhang,[c,d] Hongxia Liu,[c,d,*] and Zhigang Sun[a,c,d,*]

[a] *State Key Laboratory of Advanced Technology for Materials Synthesis and Processing, Wuhan University of Technology, Wuhan 430070, China.*

[b] *School of Science, Wuhan University of Technology, Wuhan 430070, China.*

[c] *School of Materials Science and Engineering, Taiyuan University of Science and Technology, Taiyuan 030024, China.*

[d] *Laboratory of Magnetic and Electric Functional Materials and the Applications, The Key Laboratory of Shanxi Province, Taiyuan 030024, China.*

[*] Corresponding author.

E-mail address: sun_zg@whut.edu.cn (Prof. Zhigang Sun) and hongxliu@126.com (Dr. Hongxia Liu)

Table S1 Weight ratio of nanoparticles (NPs), density (ρ), and number density of nanoparticles (N_{NP}) of composites regarding the NPs' type, size, and mole ratio.

sample name	wt%	ρ (g cm^{-3})	N_{NP} (m^{-3})
matrix		6.07	-
GT30-1	0.38	6.06	3.48×10^{20}
GT30-2	0.76	6.05	6.91×10^{20}
GT30-3	1.14	6.02	1.03×10^{21}
GT100-1	0.38	6.07	8.44×10^{18}
GT100-2	0.76	6.05	1.68×10^{19}
GT100-3	1.14	5.97	2.47×10^{19}
GF30-0.2	0.22	6.05	2.53×10^{20}
GF30-0.5	0.55	6.00	6.26×10^{20}
GF30-0.8	0.88	6.01	1.00×10^{21}
GF30-1	1.10	6.03	1.25×10^{21}
GF30-1.5	1.65	6.01	1.86×10^{21}
GF30-2	2.21	5.96	2.45×10^{21}
GF30-3	3.31	5.89	3.59×10^{21}
GF100-1	1.10	6.05	1.70×10^{19}
GF100-2	2.21	6.10	3.40×10^{19}
GF100-3	3.31	6.01	4.97×10^{19}

Table S2 Gaussian fitting values of the size distribution for the various raw nanoparticles and *d* means the diameter based on a sphere model.

raw nanoparticle	mean *d* (nm)	standard deviation (nm)	median *d* (nm)	total number	Gauss *R*-square
30 nm TiO_2	30.94	10.46	29.99	387	0.9092
100 nm TiO_2	106.95	43.95	102.61	262	0.9653
30 nm Fe_3O_4	26.86	7.30	26.19	225	0.9562
100 nm Fe_3O_4	112.62	42.09	107.64	272	0.9618

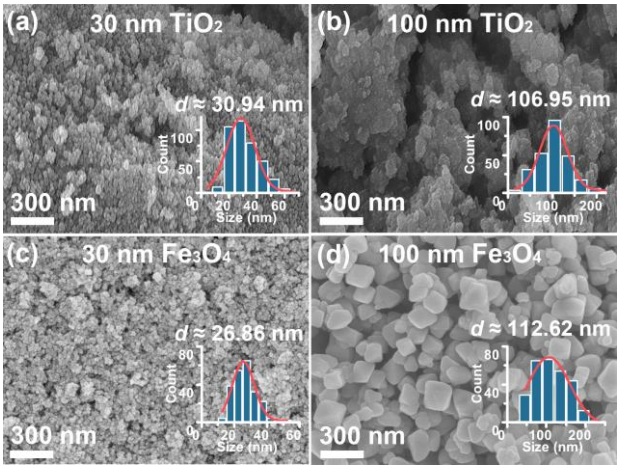

Fig.S1 SEM images of the raw (a) 30 nm TiO_2, (b) 100 nm TiO_2, (c) 30 nm Fe_3O_4, and (d) 100 nm Fe_3O_4 particles. The insets show the particle size distribution and average diameter of various raw nanoparticles.

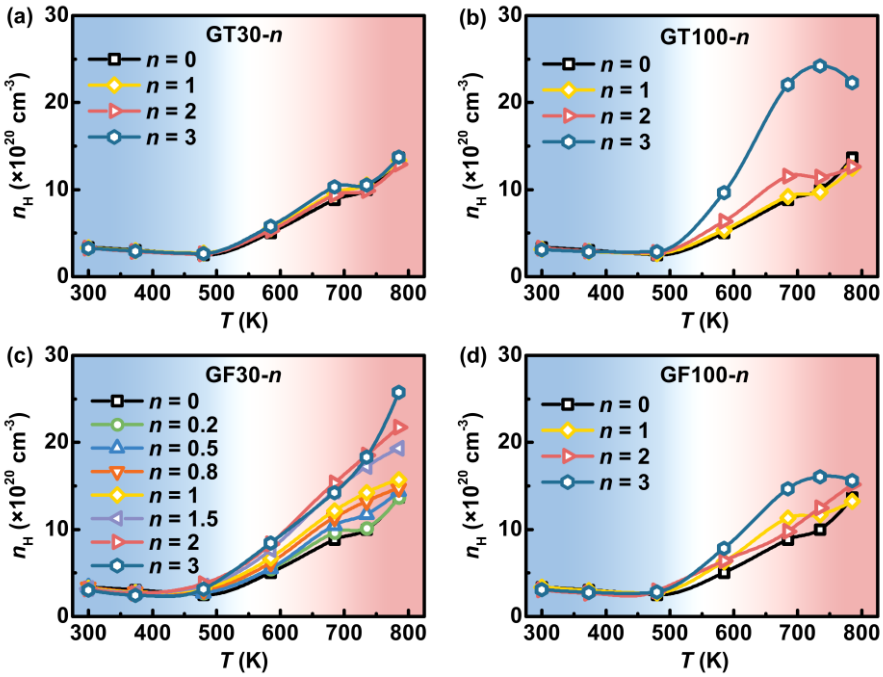

Fig.S2 Temperature-dependent carrier concentration (n_H) of (a) GT30-*n*, (b) GT100-*n*, (c) GF30-*n*, and (d) GF100-*n* composites calculated from the composites' experimental values of electrical conductivity (σ) and Seebeck coefficient (S) and the $Ge_{0.96}Bi_{0.06}Te$ matrix's assumed values of the effective mass (m^*)[1] based on the single parabolic band (SPB) model.

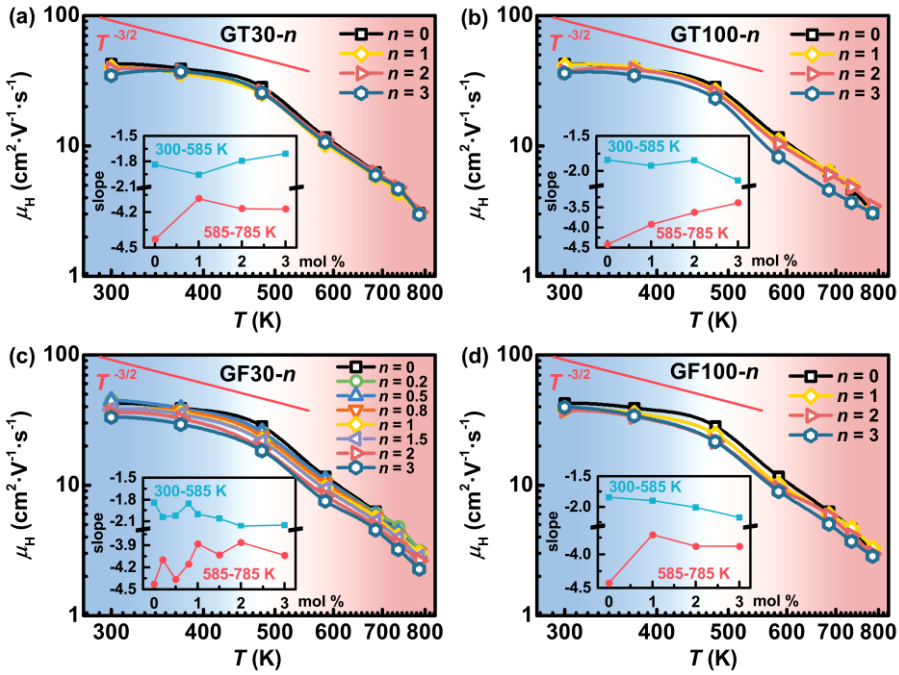

Fig.S3 Temperature-dependent logarithmic scale Hall mobility (μ_H) of (a) GT30-*n*, (b) GT100-*n*, (c) GF30-*n*, and (d) GF100-*n* composites calculated from the composites' experimental values of σ and S and the matrix's assumed values of m^{*1} based on the SPB model.

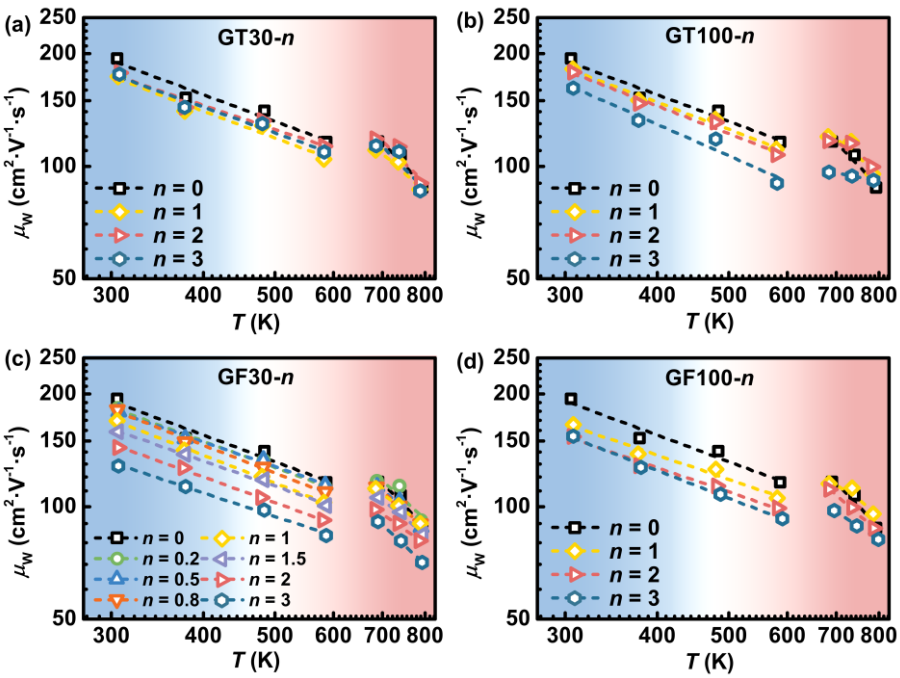

Fig.S4 Temperature-dependent logarithmic scale weighted mobility (μ_W) of (a) GT30-*n*, (b) GT100-*n*, (c) GF30-*n*, and (d) GF100-*n* composites.

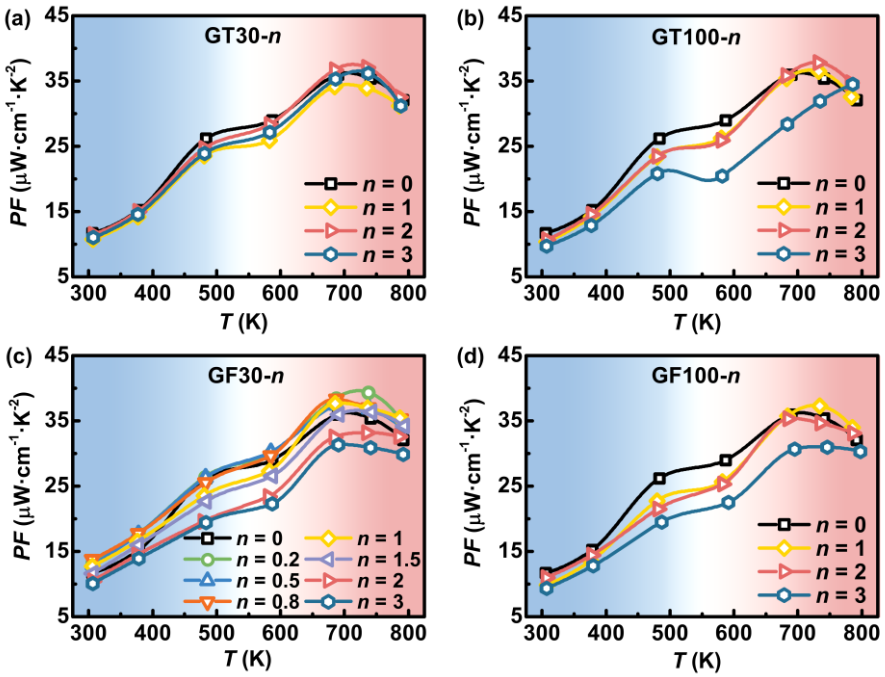

Fig.S5 Temperature-dependent power factor (*PF*) of (a) GT30-*n*, (b) GT100-*n*, (c) GF30-*n*, and (d) GF100-*n* composites.

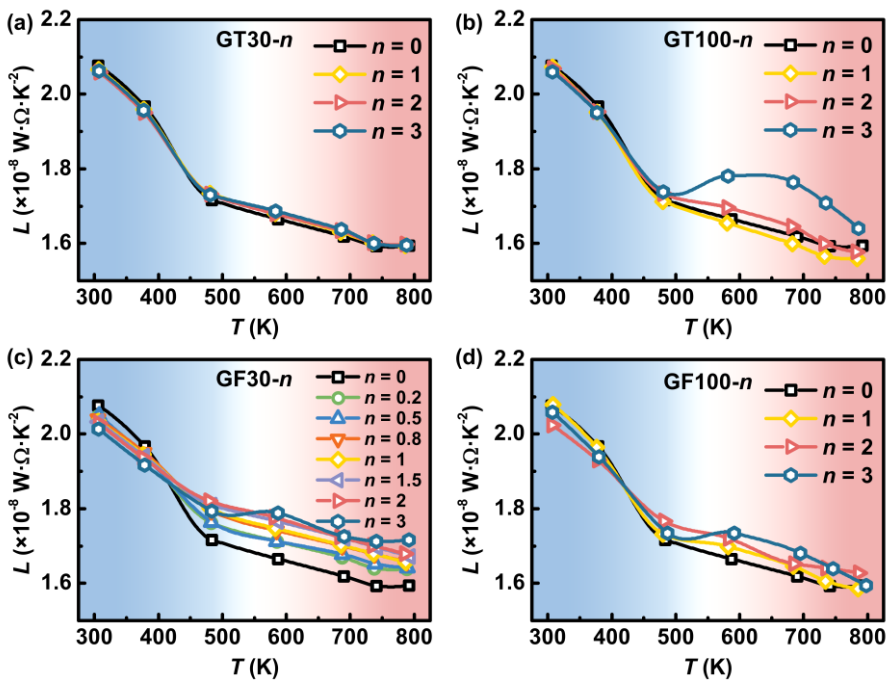

Fig.S6 Temperature-dependent Lorenz number (*L*) of (a) GT30-*n*, (b) GT100-*n*, (c) GF30-*n*, and (d) GF100-*n* composites.

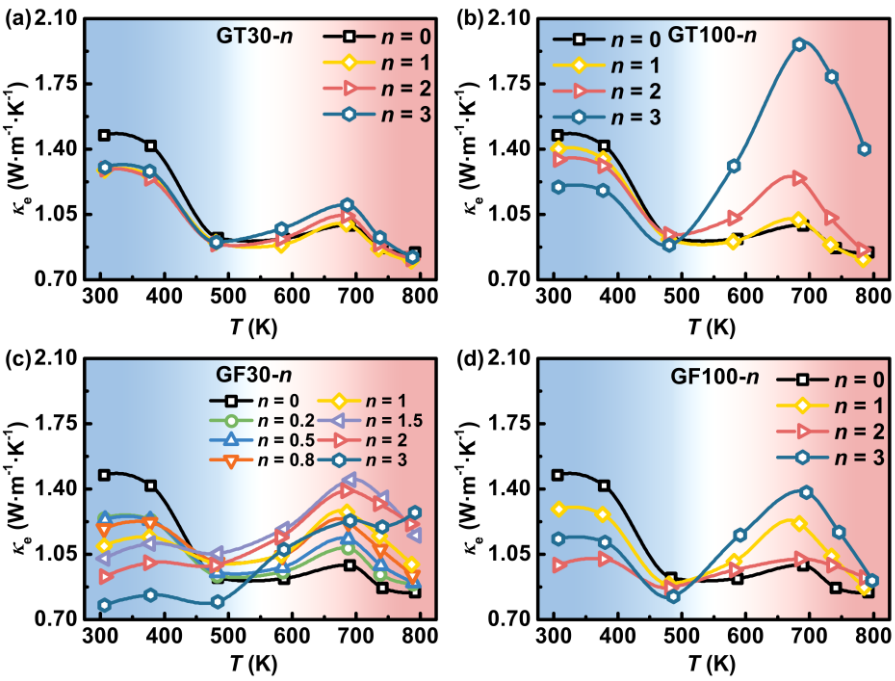

Fig.S7 Temperature-dependent carrier thermal conductivity (κ_e) of (a) GT30-*n*, (b) GT100-*n*, (c) GF30-*n*, and (d) GF100-*n* composites.

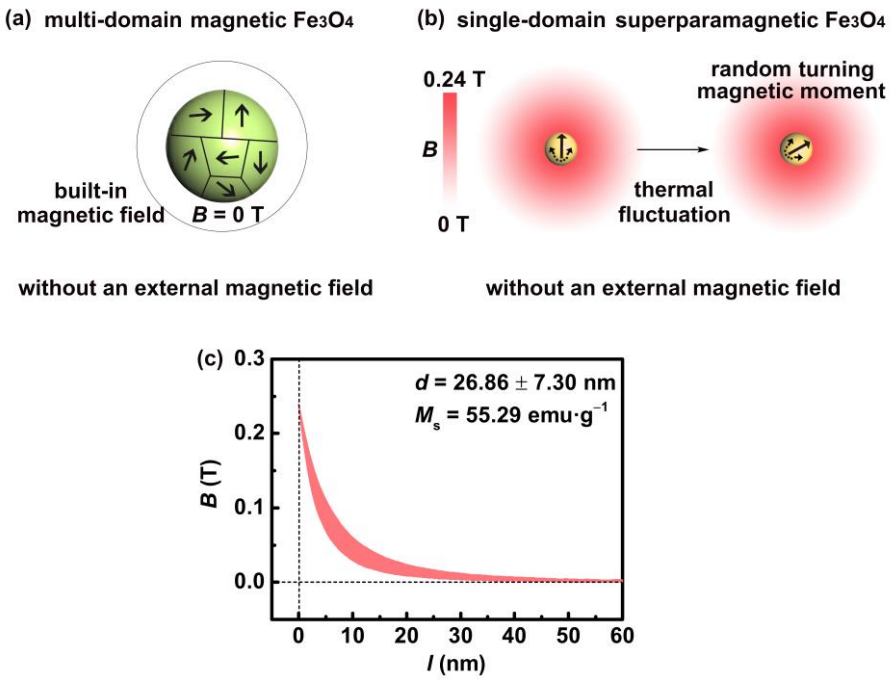

Fig.S8 Built-in magnetic field (*B*) introduced by (a) a multi-domain magnetic Fe_3O_4 nanoparticle and (b) a single-domain superparamagnetic Fe_3O_4 nanoparticle. (c) The relationship of the built-in magnetic field *B* of raw superparamagnetic Fe_3O_4 nanoparticles and the distance from their surface (*l*).

Single parabolic band (SPB) model for calculating electronic transport parameters

Utilizing the single parabolic band (SPB) model with acoustic phonon scattering, the effective mass (m^*) can be derived by:[2]

$$F_j(\eta) = \int_0^\infty \frac{\varepsilon^j}{1+\exp(\varepsilon-\eta)} d\varepsilon \tag{S1}$$

$$S = \pm \frac{k_B}{e}\left[\frac{(r+5/2)F_{r+3/2}(\eta)}{(r+3/2)F_{r+1/2}(\eta)} - \eta\right] \tag{S2}$$

$$m^* = \frac{h^2}{2k_B T}\left[\frac{n}{4\pi F_{r+1}(\eta)}\right]^{2/3} \tag{S3}$$

where $F_j(\eta)$ is the Fermi integral function and η is the reduced Fermi level ($\eta = E_F/k_BT$), and k_B and h are the Boltzmann constant and Planck constant. The scattering factor $r = -1/2$ is taken for the $Ge_{0.96}Bi_{0.06}Te$ matrix due to the phonon-dominated scattering mechanism in GeTe-based materials.[3] According to the Mott equation of the relationship between the S and n,[4]

$$S = \pm\left(\frac{8\pi^2 k_B^2}{3eh^2}\right) m^* T \left(\frac{\pi}{3n}\right)^{2/3} (r + 3/2) \tag{S4}$$

since the nanoparticles are considered to have little influence on the band structure or the crystal structure of the matrix, the m^* can be treated as a constant, and the relationship between r and S of composites can be derived as:[5]

$$\frac{(r_{\text{composite}}+3/2)}{(r_{\text{matrix}}+3/2)} = \frac{S_{\text{composite}}}{S_{\text{matrix}}}\left(\frac{n_{\text{composite}}}{n_{\text{matrix}}}\right)^{2/3} \tag{S5}$$

Then, the scattering factor of the composites can be obtained according to the values of the Seebeck coefficient and carrier concentration of the composites and the matrix.

Since both S and σ are the function of carrier concentration and are related to each other, the transport coefficients (σ_{E0}) and the weighted mobility (μ_W) are introduced to describe the intrinsic transport properties of materials.[3, 6] They can be expressed as:

$$\sigma = \sigma_{E_0} \ln(1 + e^\eta) \tag{S6}$$

$$\sigma_{E_0} = \frac{2^{9/2} e\pi (m_e k_B T)^{3/2}}{3h^3} \mu_W \tag{S7}$$

The parameter σ_{E0} is a conductivity expression independent of the carrier concentration (n_H), which excludes the error of the n_H in the Hall measurement. The σ_{E0} can be expressed by the μ_W, which is closely related to the m^*. Therefore, the change in μ_W can also explain the relationship between S and σ, and the μ_W can initially reflect the scale of PF.

The L is the Lorenz number based on the SPB approximation:[2, 7]

$$L = (\frac{k_B}{e})^2 \left\{ \frac{(r+7/2)F_{r+5/2}(\eta)}{(r+3/2)F_{r+1/2}(\eta)} - \left[\frac{(r+5/2)F_{r+3/2}(\eta)}{(r+3/2)F_{r+1/2}(\eta)} \right]^2 \right\} \quad \text{(S8)}$$

Langevin function fitting for superparamagnetic Fe_3O_4 nanoparticles

To confirm that 30 nm Fe_3O_4 NPs is indeed superparamagnetic, the experimental data of its M–H curve was fitted by the Langevin function:[5, 8, 9]

$$M = M_0(\coth\left(\frac{\mu\mu_0 H}{k_B T}\right) - \frac{k_B T}{\mu\mu_0 H}) \quad \text{(S9)}$$

where the vacuum permeability μ_0 is $4\pi \times 10^{-7}$ N·A^{-2}, the Boltzmann constant k_B is 1.38×10^{-23} J·K^{-1}, and the temperature T is 300 K. The fitting results show that the saturation magnetization intensity of 30 nm Fe_3O_4 NPs is M_0 = 54.54 emu·g^{-1}, comparable with the M_s, as shown in **Fig.4**b. And the magnetic moment of a 30 nm Fe_3O_4 NPs is $\mu = 1.12 \times 10^{-17}$ A·m^2, which is related to the average volume <V>:[5, 8, 9]

$$\mu = M_{s,bulk}\rho\langle V\rangle = M_{s,bulk}\rho\frac{\pi d^3}{6} \quad \text{(S10)}$$

where $M_{s,bulk}$ is the saturation magnetization intensity of bulk Fe_3O_4 ($M_{s,bulk}$ = 90 emu·g^{-1}).[10] Thus, the average diameter d of 30 nm Fe_3O_4 NPs obtained from the M–H curve is about 35.76 nm, close to the Gaussian analysis result of SEM (mean d = 26.86 ± 7.30 nm), as shown in **Table S2**.

Built-in magnetic field introduced by a magnetic particle

Considering the built-in magnetic field introduced by one single-domain Fe_3O_4 NP with a sphere model, the magnetic field B around the Fe_3O_4 NP can be calculated as follows[11, 12]:

$$B = \frac{2J(d/2)^3}{3(l+d/2)^3} \quad \text{(S11)}$$

where J is the saturated magnetic polarization intensity of 30 nm Fe_3O_4 ($J = \mu_0 M_s \rho = 0.36$ T), d is the diameter, and l is the distance from the sphere surface. The results are shown in **Fig.S8**c.

References:

1. C. Zhu, J. Wang, F. Luo, S. Zhang, J. Wang, Y. Zhang, H. Liu and Z. Sun, *ACS Appl. Mater. Interfaces*, 2022, **14**, 38854–38864.
2. H. Naithani and T. Dasgupta, *ACS Appl. Energy Mater.*, 2020, **3**, 2200–2213.
3. N. H. Li, W. L. He, C. J. Li, G. W. Wang, G. Y. Wang, X. Y. Zhou and X. Lu, *J. Mater. Chem. A*, 2021, **9**, 2385–2393.
4. J. Youn, J. Ryu, H. Kim, S. K. Kihoi, I.-S. Son, S.-E. Chun, S. Yi and H. S. Lee, *Appl. Phys. Lett.*, 2021, **118**, 053902.
5. W. Y. Zhao, Z. Y. Liu, Z. G. Sun, Q. J. Zhang, P. Wei, X. Mu, H. Y. Zhou, C. C. Li, S. F. Ma, D. Q. He, P. X. Ji, W. T. Zhu, X. L. Nie, X. L. Su, X. F. Tang, B. G. Shen, X. L. Dong, J. H. Yang, Y. Liu and J. Shi, *Nature*, 2017, **549**, 247–251.
6. A. Suwardi, J. Cao, Y. Zhao, J. Wu, S. W. Chien, X. Y. Tan, L. Hu, X. Wang, W. Wang, D. Li, Y. Yin, W. X. Zhou, D. V. M. Repaka, J. Chen, Y. Zheng, Q. Yan, G. Zhang and J. Xu, *Mater. Today Phys.*, 2020, **14**, 100239.
7. H.-S. Kim, Z. M. Gibbs, Y. Tang, H. Wang and G. J. Snyder, *APL Mater.*, 2015, **3**, 041506.
8. C. C. Li, S. F. Ma, P. Wei, W. T. Zhu, X. L. Nie, X. H. Sang, Z. G. Sun, Q. J. Zhang and W. Y. Zhao, *Energy Environ. Sci.*, 2020, **13**, 535–544.
9. E. C. Devi and S. D. Singh, *J. Supercond. Nov. Magn*, 2021, **34**, 617–622.
10. Y. Wei, B. Han, X. Hu, Y. Lin, X. Wang and X. Deng, presented in part at the 2011 Chinese Materials Conference, China, 2012.
11. S. Ma, C. Li, W. Cui, X. Sang, P. Wei, W. Zhu, X. Nie, F.-H. Sun, W. Zhao and Q. Zhang, *Sci. China Mater.*, 2021, **64**, 2835–2845.
12. F. Luo, C. Zhu, J. Wang, X. He, Z. Yang, S. Ke, Y. Zhang, H. Liu and Z. Sun, *ACS Appl. Mater. Interfaces*, 2022, **14**, 45503–45515.